Experimental Study of the Energy and Exergy performance for a Pressurized Volumetric Solar Receiver

Jianqin Zhu[a], Kai Wang[b,*], Zhaowu Jiang[b], Hongwei Wu[c,**],
Dunjin Wang[b], Feng Lin[b], Yongliang Li[d]

[a] National Key Lab. of Science and Technology on Aero-Engines,
School of Energy and Power Engineering, Beihang University, Beijing 100191, China

[b] Institute of Engineering Thermophysics, Chinese Academy of Sciences,
Beijing, 100190, China.

[c] Department of Mechanical and Construction Engineering, Faculty of Engineering and Environment,
Northumbria University, Newcastle upon Tyne, NE1 8ST, United Kingdom

[d] School of Chemical Engineering, University of Birmingham,
Edgbaston, Birmingham B15 2TT United Kingdom

[*]Corresponding author. Email: wang_kai@iet.cn Tel. +86(10)82543147 Fax. +86(10)82613328

[**]Corresponding author. Email: hongwei.wu@northumbria.ac.uk Tel. +44(0)1913495365

Abstract

This article presents an experimental investigation of the heat transfer characteristics as well as energy and exergy performance for a pressurised volumetric solar receiver under variable mass flow rate conditions. During a two hour period of continuous operation in the morning, the solar irradiance is relatively stable and maintained at approximately 600 W/m^2, which is beneficial for analyzing the energy and exergy performance of the solar receiver. Experimental results show that the mass flow rate fluctuation has slight effect on the solar receiver outlet temperature. Whereas the mass flow rate plays an important role in the solar receiver power, energy efficiency and exergy efficiency. The efficiency of the solar receiver is normally above 55% with the highest efficiency of 87%, and at steady state, the efficiency is maintained at around 60%. A very low value of the heat loss factor (0.014 kW/K) could be achieved during the current steady state operating conditions. The highest exergy efficiency is approximately 36%. In addition, as the temperature

difference increases, the impact of the exergy factor increases. The highest exergy factor is 0.41 during the entire test.

Keywords: solar receiver; exergy; energy efficiency; heat transfer; radiation.

Nomenclature

A_{ap}	effective aperture area of dish [m^2]	Ex_s	rate of solar exergy delivery [kw]
A_p	project area [m^2]	G	direct solar radiation [w/m^2]
c_{av}	average specific heat capacity [J/kg·K]	$\dot{m}$	mass flow rate [kg/s]
D_f	focus point diameter [m]	n_d	parabolic dish combined optical efficiency [-]
E_D	concentrated solar radiation power [kw]	r_c	concentration ratio
E_L	heat loss [kw]	T_{in}	inlet temperature of the air [K]
E_R	receiver power [kw]	T_{out}	outlet temperature of the air[K]
E_S	solar radiation power on the dish [kw]	T_{ave}	average temperature of the air[K]
Ex_D	rate of dish exergy concentrated [kw]	U_L	heat loss coefficient [kw/m^2K]
Ex_f	exergy factor [-]	$\eta_{th.R}$	energy efficiency of the receiver [-]
Ex_R	receiver exergy [kw]	$\eta_{ex.R}$	exergy efficiency of the receiver [-]

1. Introduction

With rapidly increasing energy prices and globalization, process industries seek opportunities to reduce production costs and improve energy efficiency. Among the energy-efficient technologies, Concentrated Solar Power (CSP) system is considered as one of the most attractive ways to solve the energy crisis in the future [1,2]. Many

developed countries like the United State and the European Commission have been devoted to the solarised Brayton micro-turbines system over the past decades [3-5].

Compared to the traditional gas turbine, solarised Brayton turbines use solar receiver to replace the combustion chamber in the traditional gas turbine [6]. The solar concentration part which is used to provide high temperature air is very crucial for the entire solar power system. The system efficiency and the cost of the power generation are highly depended on the solar concentration conversion efficiency from solar radiation to thermal fluid. Thus, the solar concentration part has to be well designed in order to achieve high efficiency and low pressure loss. Many studies have been devoted to the design and performance of the receiver. Neber and Lee [7] designed a high temperature cavity receiver using silicon carbide. Then a scaled test section was placed at the focal point of a parabolic dish collector and reached a maximum temperature of 1248 K. Fernandez et al. [8] presented a multidisciplinary design optimization of a 5 MW Small Particle Heat Exchange Receiver (SPHER) for a central receiver solar plants. The new developed solar receiver aims to heat air to temperatures in excess of 1300 K and use this high-temperature energy to drive a Brayton cycle or a combined Brayton/Rankine cycle. It was found that the receiver efficiency can be increased by 6% with respect to the previous baseline design from the same author [9]. Buck et al. [10] introduced a receiver module consisting of a secondary concentrator and a volumetric receiver unit which was closed with a domed quartz window to transmit the concentrated solar radiation. Hischier et al. [11, 12]

proposed a novel design of a high-temperature pressurized solar air receiver for power generation via combined Brayton-Rankine cycles. It consists of an annular reticulate porous ceramic bounded by two concentric cylinders. The heat transfer mechanism was analyzed by the finite volume technique and by using the Rosseland diffusion, P1, and Monte-Carlo radiation method. It was found that, for a solar concentration ratio of 3000 suns, the outlet air temperature can reach 1000 °C at 10 bars, yielding a thermal efficiency of 78%.

It is recognized that the flow and heat transfer processes in the solar receiver are very complicated. Over the past years, many studies have been devoted to the optimization of the design using theoretical and numerical method. Cui et al. [13] developed a three-dimensional optical model and simulated the solar transmission process for a pressurized volumetric receiver using the Monte Carlo Ray Tracing (MCRT) method. Wang et al. [14] developed a three-dimensional model of parabolic dish-receiver system with argon gas as the working fluid to simulate the thermal performance of a dish-type concentrated solar energy system. Lu et al. [15] proposed heat and mass transfer models of the solar heat receiver, and associated heat absorption and exergetic performance were further investigated by considering the heat loss outside the receiver and fluid viscous dissipation inside the receiver. Song et al. [16] analyzed the effect of the solar incidence angle in order to accurately simulate the heat flux distribution around the absorber tube outer surface. Le Roux et al. [17] investigated the effect of wind, receiver inclination, rim angle, atmospheric

temperature and pressure, recuperator height, solar irradiance and concentration ratio on the optimum geometries and performance. Lu et al. [18] theoretically investigated the nonuniform heat transfer model and performance of parabolic trough solar receiver and the results showed that the heat loss of solar receiver from the nonuniform model is a slight higher than that from the uniform model.

On the other hand, many numerical research works are also conducted to simulate the detail heat transfer process. Flesch et al. [19] numerically analyzed the impact of head-on and side-on wind on large cavity receivers with inclination angles ranges from 0° (horizontal cavity) to 90° (vertical cavity) and compared with the data published in the open literature. Wei et al. [20] presented an original CFD-based evolutionary algorithm to determine the optimal fluid distribution in a tubular solar receiver for the minimization of its peak temperature. Tu et al. [21] proposed a modified combined method to simulate the thermal performance of a saturated water/steam solar cavity receiver. Capeillere et al. [22] numerically studied the thermomechanical behavior of a plate solar receiver with asymmetric heating. The numerical results showed that the choice of the shape and levels of the solar irradiance map is crucial. The distribution of the most relevant incident solar flux and the geometry compromise were determined. Wang et al. [23] conducted a numerical study focusing on the thermal performance of porous medium receiver with quartz window. Their results indicated that the pressure distribution and temperature

distribution for the condition of fluid inlet located at the side wall was different from that for the condition of fluid inlet located at the front surface.

Exergy analysis has been applied in various power studies [24-26]. Thermodynamic analyses and optimization of a recompression N_2O Brayton power cycle have been performed [27]. The performance of a regenerative Brayton heat engine has been studied by focusing on the minimization of irreversibility [28]. In the authors' earlier studies [29, 30], a coiled tube solar receiver has been designed and tested in the real solar radiation condition. But due to the limitation of the tube material, the coiled tube solar receiver can not achieve very high temperature. Thus, a pressurized volumetric solar receiver using metal foam as thermal absorbing core is designed in this work. It appears from the previous investigation that the key point for the solarised Brayton micro-turbines is to develop solar receivers which have terrific performance on the pressure loss and heat transfer. To the best of the authors' knowledge, there is a lack of available experimental data under real concentrate solar and variable mass flow conditions especially for the cases of extremely high heat flux and high temperature. To this end, the present research is aimed to experimentally analyze both the efficiency and heat loss of a pressurized volumetric solar receiver under real solar radiation and variable mass flow conditions in more detail.

2. Experimental apparatus and method

2.1. Experimental apparatus

The experimental study was conducted at a location with the geographical position of 30°36' latitude and 120°22' longitude, Hangzhou, China. The whole system, shown schematically in Fig. 1, mainly consists of three components: dish, compressor and receiver. The dish used for the experimental tests of the developed solar heat receiver was listed in Fig. 2. All 40 trapezoidal, pre-bent mirrors are resin molded and laminated. The reflective surface is applied as an adhesive foil. At the bottom of the dish a cut out is made for the tower. The main dish parameters utilized in the current study are illustrated in Table 1, which is provided by the dish reflector manufacturer. To make sure that the light reflected by the mirror focus on the aperture of the receiver, each mirror was adjusted carefully.

The dish is controlled by a solar tracker which is embedded in the inner program to make the dish face the Sun automatically. The inner program could accurately calculate the attitude angle in terms of the dish location of the earth and the local time. As illustrated in Fig. 1, the attitude angel is formed between the boom line and horizon line. A stepping motor can be well controlled to change the dish attitude angle slowly. When the dish is in operation during the morning, the attitude angle is lower than $40°$ for the sun just rising over the horizontal line. Whereas the dish is operated in the noon, the attitude angle is approximately $80°$. It should be recognized that the initial setting for the location and accurate time is very crucial during the test. An uninterruptible power supply (UPS) system is also adopted to assist the dish off the solar direction in some emergency to further protect the receiver. During the

experiments, a 20 kw piston compressor driven by the electricity is used to compress the air. The pressurized air is compressed at environmental temperature and pressure. After the filter, the air is pressurized into the air tank with the pressure of 0.8 Mpa to guarantee the enough air flow during the experiment process. After that the pressurized air is supplied into the receiver. Two valves are installed at the receiver inlet and outlet to ensure the receiver works under designed pressure about 0.4 Mpa. Because the light incident surface of the receiver is made of quartz glass, too high pressure could damage the receiver. Hence, by adjusting this valve, the pressure of the whole system as well as the portion of the receiver can be well controlled. The output mass flow rate is variable. Thermocouple and pressure sensor are placed at the inlet and outlet of the pipe respectively to obtain the receiver efficiency and heat loss. The receiver itself is mounted onto the cantilever arm. In the current study, the heat flux of the focus power could achieve 1000 kW/m^2 for the dish concentrator has the concentrate ratio of 1750. It can be expected that, except for the receiver and protecting panel, other components of the system would be burned in a short time. To protect other part of the receiver from misaligned radiation an additional protecting panel is mounted circumferentially to the receiver. As shown in Fig. 3, the protecting panel is made of Calcium silicate board with 10 mm in thickness. The diameter of the aperture in the protecting panel is 250 mm. Four K-type thermocouples with an accuracy of 0.5 ℃ are fixed on the back to monitor the temperature of the protecting panel. When the temperature is over 850 ℃, it means that the concentrate solar spot is

not located into the aperture. As a result, the inner program has to be reset to adjust the attitude angle in order to prevent fatal damage.

2.2. Solar receiver model

For the current experimental evaluation, as shown in Fig. 4, the solar receiver is designed as a type of pressurized volumetric solar receiver. Fig. 4(a) shows the 3D view of the model and Fig. 4(b) presents the cross sectional view of the receiver. The advantage of the pressurized volumetric solar receiver is high outlet air temperature and high thermal efficiency. It should be stressed here that the key point for the design of the pressurized volumetric solar receiver is the cooling of the light incident glass and the equally distributed mass flow in the heat absorbing core. The light incident glass is made of quartz glass which can endure a temperature up to 1500 C°. But the concentrated solar focuses on the quartz glass directly, the glass cooling using the inlet air could extend the life span of the receiver and make the receiver working process more secure. For this reason, a big inlet tube is used with the diameter of 50 mm. The pressured air is injected into the inlet tube, and then, it is divided into three small tubes with the diameter of 20 mm. The three small tubes that circumferentially uniformly distributed are welded at the end of the pressure cavity which forms the main part of the solar receiver. The air flow along the edge of the cavity and inject on the quartz glass forming the cooling of the light incident glass. The diameter and the height of the main part of the receiver are 400 mm and 360 mm, respectively. The concentrate solar radiation (CSR) passes through the quartz glass and heat the

absorbing core. As shown in Fig. 5, the material of the absorbing core is Nickel foam which could endure the temperature up to 1453 ℃. To increase the absorbing ability, 65mm Nickel foam with the PPI (Pores per Inch) value of 75 is selected. PPI which is a common parameter is usually used in industry to indicate the pore diameter of the metal foam. The 75 PPM value means that the pore diameter is about 0.34 mm. One can imagine that the small pore diameter would enhance the heat transfer coefficient and heat transfer area easily. At last, to minimize the heat loss, the receiver is surrounded by Aluminum silicate whose heat conductivity coefficient is $0.06\ \mathrm{W/m^2\ K^{-1}}$.

2.3. Energy and exergy analysis

Experimental energy and exergy parameters to characterize the thermal performance of the receiver are presented in this section.

2.3.1. Energy analysis [31, 32]

The energy that the whole system receives comes from the solar radiation. The solar radiation power on the parabolic dish reflector can be expressed as:

$$\mathrm{E_S} = \mathrm{A_{ap}G} \quad (1)$$

where $\mathrm{E_S}$ is the solar radiation power on the dish, A_{ap} is the effective aperture area of the parabolic dish, and *G* is the direct solar irradiation from the Sun to the dish. *G* is measured with a normal incidence pyrheliometer (NIP) Hukseflux DR01 attached to the solar tracker.

The solar radiation is concentrated and delivered to the receiver by the parabolic dish. The concentrated solar radiation power (E_D) can be expressed as:

$$E_D = n_d E_S = n_d A_{ap} G \quad (2)$$

where E_D is the concentrated solar radiation power from parabolic dish to the receiver, n_d is the parabolic dish combined with optical efficiency described in Table 1.

The concentrated solar radiation on the receiver is absorbed by the heat-transfer fluid flowing in the pressurized cavity of the receiver. The energy rate that air absorbs or receives power is given by:

$$E_R = \dot{m} c_{av} (T_{out} - T_{in}) \quad (3)$$

where $\dot{m}$ is the mass flow rate of the air, c_{av} is the average specific heat capacity of the air which is a function of the average air inlet temperature (T_{in}) and air outlet temperature (T_{out}). The average temperature of the receiver (T_{ave}) can be defined by:

$$T_{ave} = (T_{in} + T_{out})/2 \quad (4)$$

Thus, the relation between the average specific heat capacity of the air and the average temperature can be obtained as:

$$c_{av} = 0.9956 + 0.000093 T_{ave} \quad (5)$$

Based on the energy conservation, the receiver power is the difference between the concentrated solar radiation power and the overall heat losses are relative low. The receiver power can also be described as

$$E_R = E_D - E_L \quad (6)$$

where E_L is the rate of the heat loss from the receiver to the surroundings, which contains the convective heat losses, conductive heat losses and radioactive heat losses. E_L can be expressed as

$$E_L = U_L A_R (T_{ave} - T_{amb}) \quad (7)$$

where U_L is the total heat loss coefficient determined, A_R is the effective receiver area, and T_{amb} is the ambient temperature. The product $U_L A_R$ is referred as the heat loss factor given by

$$U'_L = U_L A_R \quad (8)$$

Therefore, combination of Eqs (2), (3), (6) and (7) can yield

$$\dot{m} c_{av} (T_{out} - T_{in}) = n_d A_{ap} G - U'_L (T_{ave} - T_{amb}) \quad (9)$$

The thermal energy efficiency of the receiver is defined as the ratio of the receiver power to the concentrated solar radiation power from the parabolic dish to the receiver which is expressed as:

$$\eta_{th.R} = \frac{E_R}{E_D} = \frac{\dot{m} c_{av} (T_{out} - T_{in})}{n_d A_{ap} G} \quad (10)$$

By dividing $A_{ap} G$ on both side of Eq. (9) and combine with Eq. (10) leads to

$$\eta_{th.R} n_d = n_d - \frac{U'_L (T_{ave} - T_{amb})}{A_{ap} G} \quad (11)$$

2.3.2 Exergy analysis [31, 32]

The exergy rate of the receiver or the quality of the energy delivered to the circulating fluid with reference to the surroundings can be expressed as

$$Ex_R = E_R - \dot{m}c_{av}T_{amb}\ln\left(\frac{T_{out}}{T_{in}}\right) \quad (12)$$

Substituting Eq. (3) into Eq. (12) yields

$$Ex_R = \dot{m}c_{av}\left[(T_{out} - T_{in}) - T_{amb}\ln\left(\frac{T_{out}}{T_{in}}\right)\right] \quad (13)$$

The rate of the solar exergy delivery by the Sun to the dish and then to the concentrator is given by the Petela expression [33] and is expressed as

$$Ex_s = GA_{ap}\left[1 + \frac{1}{3}\left(\frac{T_{amb}}{T_s}\right)^4 - \frac{4T_{amb}}{3T_s}\right] \quad (14)$$

where T_s is the surface temperature of the Sun which is approximately 5762 K.

So the concentrated solar radiation exergy (Ex_D) can be expressed as:

$$Ex_D = n_d GA_{ap}\left[1 + \frac{1}{3}\left(\frac{T_{amb}}{T_s}\right)^4 - \frac{4T_{amb}}{3T_s}\right] \quad (15)$$

The exergy efficiency is defined as the ratio of the receiver exergy rate to the rate of the concentrated solar radiation exergy and can be determined as follows:

$$\eta_{ex.R} = \frac{Ex_R}{Ex_D} = \frac{\dot{m}c_{av}\left[(T_{out}-T_{in})-T_{amb}\ln\left(\frac{T_{out}}{T_{in}}\right)\right]}{n_d GA_{ap}\left[1+\frac{1}{3}\left(\frac{T_{amb}}{T_s}\right)^4-\frac{4T_{amb}}{3T_s}\right]} \quad (16)$$

The exergy factor is defined as the ratio of the receiver exergy rate to the receiver energy rate and can be represented by equation:

$$Ex_f = \frac{Ex_R}{E_R} = \frac{\dot{m}c_{av}\left[(T_{out}-T_{in})-T_{amb}\ln\left(\frac{T_{out}}{T_{in}}\right)\right]}{\dot{m}c_{av}(T_{out}-T_{in})} \quad (17)$$

3. Uncertainty analysis

The uncertainties of the measurement in the experiment are dependent on the experimental conditions and the measurement instruments. An uncertainty analysis is

performed on the receiver power E_R and the receiver exergy Ex_R, which are the most important derived quantities from the measurements of using the propagation of error method described by Moffat [34]. The uncertainty of the receiver power could be calculated by the following equation:

$$\delta E_R = \sqrt{\left(\frac{\delta E_R}{\delta \dot{m}}\right)^2 (\delta \dot{m})^2 + \left(\frac{\delta E_R}{\delta T_{out}}\right)^2 (\delta T_{out})^2 + \left(\frac{\delta E_R}{\delta T_{in}}\right)^2 (\delta T_{in})^2} \quad (17)$$

While the uncertainty of the receiver exergy rate is given by

$$\delta Ex_R = \sqrt{\begin{matrix}\left(\frac{\delta Ex_R}{\delta \dot{m}}\right)^2 (\delta \dot{m})^2 + \left(\frac{\delta Ex_R}{\delta T_{out}}\right)^2 (\delta T_{out})^2 \\ + \left(\frac{\delta Ex_R}{\delta T_{in}}\right)^2 (\delta T_{in})^2 + \left(\frac{\delta Ex_R}{\delta T_{amb}}\right)^2 (\delta T_{amb})^2\end{matrix}} \quad (18)$$

In the current study, the main uncertainty parameters are the mass flow rate ($\dot{m}$), the inlet temperature (T_{in}), and the outlet temperature (T_{out}). The relative uncertainty of the mass flow rate is given by the float flowmeter with the value of 2%. Therefore, $\delta \dot{m} = 2\% \times \dot{m} = \pm 0.001\ kg/s$. The uncertainty of the temperature is given by the K-type thermocouple with the value of $\delta T_{out} = \delta T_{in} = \pm 0.5\ K$.

The maximum experimental values for the receiver power and exergy rate are around 18.5 kW and 7.28 kW, respectively. The uncertainty of the receiver power is 0.372 kW, and the uncertainty of the receiver exergy rate is 0.147 kW. Overall, the overall uncertainty of the receiver power and exergy rate are 2.01% and 2.02%, respectively.

4. Results and discussion

Fig. 6 shows the variation of the solar irradiance (G) during a test period from 10:00 am to 13:30 pm. The experimental data were collected on November 6th, 2015,

291 which is a local autumn season in Hangzhou, China. According to Fig. 6, it is shown
292 that the solar irradiance fluctuates at around 600 W/m^2 all the time. And the solar
293 irradiance data increases slowly with time except two fast drops observed in the
294 afternoon for about 15 mins. The reason could be due to the fact that two short period
295 of passing cloud occurred. From this figure, it can be seen clearly that the solar
296 irradiance is almost stable and maintained at around 600 W/m^2 from 10:00 am to
297 12:00 pm. It is obviously that the stable solar irradiation condition is beneficial for
298 analyzing the energy and exergy performance of the solar receiver. For this purpose, a
299 test period of continuous 2 h from 10:00 am to 12:00 pm is selected. Dynamic
300 acquisition system is used to record the parameters automatically during the test. The
301 ambient temperature is maintained at around 25 ℃ during the experiment process.
302 Fig. 7 shows the variation of the inlet pressure, outlet pressure and mass flow rate. For
303 the design pressure of the solar receiver is 0.4 Mpa, the experiment should be
304 conducted at the same pressure. Since the heating from the concentrate solar
305 irradiation could lead to the rising of the internal pressure, the inlet valve is adjusted
306 during the experimental process to ensure the solar receiver working safety. Therefore,
307 the mass flow rate fluctuates all the time. The average value of the mass flow rate is
308 about 0.036 kg/s. In the current study, the main purpose is to test the energy and
309 exergy performance of the solar receiver under the fluctuant mass flow rate condition.
310 Fig. 8 presents the time series of air temperatures at the inlet and outlet of the
311 receiver. The inlet temperature maintains nearly constant about 42 ºC. The outlet

312 temperature rises very quickly at the starting stage, and achieves the highest
313 temperature of 480 ^{o}C at the end of the experiment process. From 10:00 am to 10:30
314 am, it takes about half an hour to rise the solar receiver outlet temperature from 42 ^{o}C
315 to 430 ^{o}C. After 10:30 am, the outlet temperature increases very slowly with the time.
316 The first half an hour is used for preheating. It is due to the fact that the receiver tubes
317 are surrounded by the insulation materials with high specific heat capability (*Cp*). It is
318 noteworthy that the rising speed of the receiver efficiency is very high within the first
319 30 mins. This phenomenon is very important and should be stressed here since the
320 sunshine is limited in the day time, quick start up can make the overall solar power
321 generation system to generate more electricity. Therefore, the cost of the power
322 generation will be lower and the investment recovery period could be shorter. There is
323 also another interesting phenomenon that the mass flow rate fluctuation has little
324 effect on the solar receiver outlet temperature. It may be due to the reason that the
325 porous metal is used as the heat absorbing core. The pore size is very small with the
326 value about 0.34 mm. This small size pore could increase the heat transfer coefficient
327 and area obviously. The heat transfer between the porous metal and the air is strong
328 enough that the air outlet temperature could be very close to the temperature of the
329 porous metal. Therefore, the effect of the mass flow rate fluctuation on the solar
330 receiver outlet temperature is very small.

331 Fig. 9 presents a comparison of the power for the concentrated solar radiation
332 and receiver power. For the case of the nearly constant solar irradiance of 600 W/m^2,

333 the concentrated solar radiation power (E_D) is maintained at around 22.5 kW with the
334 fluctuation lower than $\pm 10\%$. In addition, the accurate control system can make sure
335 the reflection focus located at the aperture of the receiver. The red line shown in Fig.
336 9 is the receiver power during the testing period. At the first 10 mins, the solar
337 receiver power (E_R) rise quickly from nearly 0 kW to 12 kW. After that, the value of
338 E_R has the same trend with the mass flow rate according to the time. In other words,
339 the mass flow rate has great influence on the solar receiver power. This can be easily
340 explained by the Eq. (3). As previously mentioned, the mass flow fluctuation has little
341 influence on the value of c_{av}, T_{out} and T_{in}, so the solar receiver power is mainly
342 affected by the mass flow rate especially after the starting stage. The maximum solar
343 receiver power is achieved at about 11:50am with the value of 18.5 kW.

344 Fig. 10(a) shows the time series of the solar receiver efficiency. It is found that
345 when the solar receiver turns into steady state, the efficiency of the solar receiver can
346 be above 55%. The peak value of the efficiency is 87%, and finally, the efficiency is
347 maintained at around 60%. And it is also found that the value of $\eta_{th.R}$ has the same
348 trend with the mass flow rate after the receiver entering into steady stage. In other
349 words, the energy efficiency is positively related with the mass flow rate as shown in
350 Fig. 10(b). The main reason for this phenomenon can be explained by Eq. (10). As
351 described above, the concentrated solar radiation power (E_D) is nearly maintained
352 constant at around 22.5 kW, but the mass flow rate has great influence on the solar
353 receiver power (E_R). Therefore, the ratio of E_R and E_D has the positive

relationship with the mass flow rate. This is a very beneficial conclusion. Because in out experiment, the mass flow rate is obviously lower than the real solarised gas turbine system. So the efficiency of the real solarised gas turbine system will be very high. Correspondingly, the usage of the gas will be lower and the investment recovery period could be shorter.

Fig. 11 demonstrates the evolution of the heat loss factor (U_L'). At the starting point, U_L' is very high (1.17 kW/K) because of the receiver preheating, and then it drops very quickly within the first 5 mins. When the receiver works at steady state, the heat loss becomes lower and U_L' achieves the minimum value of 0.014 kW/K. In the current study, the heat loss mainly consist of the conduction heat loss, conviction heat loss and radioactive heat loss. Conduction heat loss could be reduced by using material with low thermal conductivity. In the present work, the receiver is surrounded by Aluminum silicate whose thermal conductivity is 0.06 $\mathrm{W/m^2\,K^{-1}}$. The Aluminum silicate can be acted as the thermal insulator to minimize the heat loss.The thermal convection between the solar receiver and ambient is very low as well, this is because the absorbing core is sealed in a pressurized cavity. As a result, only small natural convection occurs around the external cavity of the receiver. It is noted that the use of the insulator could obviously reduce the natural convection. The radioactive heat loss is also an important part of the heat loss, but it can be reduced by using small aperture, as shown in Fig 4. In the design of solar receiver, choosing appropriate aperture diameter is very important for the receiver performance.

Fig. 12 shows the comparison between the receiver exergy (Ex_R) and the concentrated solar energy as well as the receiver energy. From this figure, the exergy rate and energy rate vary in a similar manner, the mass flow rate also has the same influence on the exergy rate. It is noted that the highest value of the exergy rate during the test period is around 7.28 kW, whereas the maximum energy rate can reach 18.5 kW. It can be concluded that the quality of the energy from the receiver is low due to a large amount of irreversible energy changes such as heat losses and the transfer of high quality solar energy to a fluid that circulating at a relatively low temperature. From Eq. (13), it can be concluded that under the same temperature difference$(T_{out} - T_{in})$ and the same energy rate $\dot{m}c_{av}(T_{out} - T_{in})$ condition, increasing the receiver inlet temperature (T_{in}) can achieve higher exergy rate (Ex_R). This will be very helpful for the design of the solar power system. As a result, some recuperator or heat exchanger should be used in the inlet of the solar receiver to recover the waste heat and increase the solar inlet temperature.

Fig. 13 presents the comparison between the energy efficiency and exergy efficiency. It is shown from Fig. 13 that similar trends in the exergy efficiency and the energy efficiency are obtained. The highest exergy efficiency is approximately 36%, whereas the highest energy efficiency is around 87%. This suggests that low quality energy obtained from the receiver. It is because the inlet temperature of the receiver is lower than 316 K, whereas the outlet temperature is very high and with the maximum value of 850 K. The temperature ratio (T_{out}/T_{in}) is very high so that too much exergy

loss is observed. Therefore, increasing the inlet temperature could be a potential way to increase the exergy efficiency.

Fig.14 shows the exergy factor plotted as a function of the temperature difference between the outlet and inlet temperature of the receiver with a linear fitting equation. The exergy factor is also usually used as a measure of the performance of the receiver. Obviously, as the temperature difference increases, the exergy factor also increases. This plot suggests that the higher exergy factor can be obtained when high temperature difference is available. As seen from this figure, the highest exergy factor is 0.41 during the entire test.

5. Conclusions

This paper performed an experimental study to investigate the thermal performance of a pressurized volumetric solar receiver under real solar radiation condition. The mass flow rate is variable during the experimental process. A parabolic dish with solar tracker system is designed and analysed using energy and exergy analyse method. Experimental results reveal that the solar irradiance is almost stable and maintained at around 600 W/m^2 from 10:00 am to 12:00 pm. It takes about half an hour to rise the solar receiver outlet temperature from 42 ^oC to 430 ^oC. After 10:30 am, the outlet temperature increases very slowly with the time. The mass flow rate fluctuation has little effect on the solar receiver outlet temperature. However, the mass flow rate has great influence on the solar receiver power, energy efficiency and exergy efficiency. The efficiency of the solar receiver can be above 55%. The peak

value of the efficiency is 87%, and finally, the efficiency is maintained at around 60%. During the steady state, the heat loss becomes lower and U_L' achieves the minimum value of 0.014 kW/K. The highest exergy efficiency is approximately 36%, whereas the highest energy efficiency is around 87%. As the temperature difference increases, the impact of the exergy factor increases. The highest exergy factor is 0.41 during the entire test.

Acknowledgements

The authors would like to acknowledge the financial support from National Natural Science Foundation of China (No. 51206164).

References

[1] Steinfeld A. 2005. Solar thermochemical production of hydrogen - a review. Solar Energy, 78:603-15.

[2] Le Roux WG, Bello-Ochende T, Meyer JP. 2011. Operating conditions of an open and direct solar thermal Brayton cycle with optimised cavity receiver and recuperator. Energy, 36:6027-36.

[3] Uri Fisher, Chemi Sugarmen, Arik Ring, Joseph Sinai, 2004. Gas Turbine "Solarization"-Modifications for Solar/Fuel Hybrid Operation, J. Sol. Energy Eng. 126(3), 872-878

[4] Peter Heller, Markus Pfänder, Thorsten Denk, Felix Tellez, Antonio Valverde, Jesús Fernandez, Arik Ring, 2006. Test and evaluation of a solar powered gas turbine system, Solar Energy, 80(10), 1225-1230

[5] Peter Schwarzbözl, Reiner Buck, Chemi Sugarmen, Arik Ring, Ma Jesús Marcos Crespo, Peter Altwegg, Juan Enrile, 2006. Solar gas turbine systems: Design, cost and perspectives, Solar Energy, 80(10), 1231-1240

[6] Chen Lingen, Zhang Wanlin, Sun Fengrui, 2007. Power efficiency entropy-generation rate and ecological optimization for a class of generalized irreversible universal heatengine cycles. Appl. Energy, 84:512-25.

[7] Matthew Neber, Hohyun Lee, 2012. Design of a high temperature cavity receiver for residential scale concentrated solar power. Energy, 47:481-487

[8] Fernandez P., Miller F. J., 2015. Performance analysis and preliminary design optimization of a small particle heat exchange receiver for solar tower power plants, Solar Energy, 112:458-68.

[9] Fernandez, P., 2013. Numerical-Stochastic Modeling, Simulation and Design Optimization of Samll Particle Solar Receviers for Concentrated Solar Power Plants. Proyecto Fin de Carrera, University of Valladolid, Span.

[10] Buck R, Brauning T, Denk T, Pfander M, Schwarzbozl P, Tellez F. 2001. Solar-hybrid gas turbine-based power tower systems, J. Sol. Energy Eng. 124(1):2-9.

[11] Hischier I., Hess D., Lipinski W., Modest M., Steinfield A., 2009. Heat transfer analysis of a novel pressurized air receiver for concentrated solar power via combined cycles. J. Thermal Sci. Eng. Appl. 1:1-6.

[12] Hischier I., Hess D., Lipinski W., Modest M., Steinfield A., 2009. Heat transfer analysis of a novel pressurized air receiver for concentrated solar power via combined cycles. ASME, Vol. 1 / 041002-1.

[13] Cui F.Q., He Y.L., Cheng Z.D., Li D., Tao Y.B., 2012, Numerical simulations of the solar transmission process for a pressurized volumetric receiver, Energy, 46:618-628

[14] Wang M., Siddiqui K., 2010. The impact of geometrical parameters on the thermal performance of a sola receiver of dish-type concentrated solar energy system. Renew. Energy, 35:2501-13.

[15] Lu J., Ding J., Yang J., Yang X., 2012. Exergetic optimization for solar heat receiver with heat loss and viscous dissipation, Solar Energy, 86: 2273-81.

[16] Song Xingwang, Dong Guobo, Gao Fangyuan, Diao Xungang, Zheng Liqing, Zhou Fuyun, 2014, A numerical study of parabolic trough receiver with no-uniform heat flux and helical screw-tape inserts, Energy, 77:771-782

[17] Le Roux W.G., Bello-Ochende T., Meyer J.P., 2011, Operating conditions of an open and direct solar thermal Brayton cycle with optimized cavity receiver and recuperator, Energy, 36:6027-6036

[18] Jianfeng Lu, Jing Ding, Jianping Yang, Xiaoxi Yang, 2013, Nonuniform heat transfer model and performance of parabolic trough solar receiver, Energy, 59:666-675

[19] Flesch R., Stadler H., Uhlig R., 2014. Numerical analysis of the influence of inclination angle and wind on the heat losses of cavity receivers for solar thermal power towers, Solar Energy, 110:427-37.

[20] Min Wei, Yilin Fan, Lingai Luo, Gilles Flamant, 2015. Fluid flow distribution optimization for minimizing the peak temperature of a tubular solar receiver, Energy, 91:663-677

[21] Tu N., Wei J., Fang J., 2015. Numerical investigation on uniformity of heat flux for semi-gray surfaces inside a solar cavity receiver, Solar Energy, 112:128-43.

[22] Capeillere J., Toutant A., Olalde G., Boubault A., 2014. Thermomechanical behavior of a plate ceramic solar receiver irradiated by concentrated sunlight, Solar Energy, 110: 174-87.

[23] Wang F., Tan J., Ma L., Shuai Y., Tan H., Leng Y., 2014. Thermal performance analysis of porous medium solar receiver with quartz window to minimize heat flux gradient, Solar Energy, 108: 348-59.

[24] Torres Reyes E, Picon Nunez M, Cervantes de GJ. 1998. Exergetic analysis and optimization of a solar-assisted heat pump. Energy, 23(4):337e44.

[25] Ameri M., Behbahaninia A., Abbas Tanha A., 2010. Thermodynamic analysis of a tri-generation system based on micro-gas turbine with a steam ejector refrigeration system. Energy, 35:2203-9.

498 [26] Blanco-Marigorta AM, Victoria Sanchez-Henríquez M, Peña-Quintana JA. 2011,
499 Exergetic comparison of two different cooling technologies for the power cycle
500 of a thermal power plant. Energy, 36:1966-72.
501 [27] Sarkar J. 2010. Thermodynamic analyses and optimization of a recompression
502 N_2O Brayton power cycle. Energy, 35:3422-8.
503 [28] Wu C, Chen L, Sun F., 1996, Performance of a regenerative Brayton heat engine.
504 Energy, 21(2):71-6.
505 [29] Jianqin Zhu, Kai Wang, Hongwei Wu, Dunjin Wang, Juan Du, A.G.Olabi,
506 Experimental investigation on the energy and exergy performance of a coiled
507 tube solar receiver, Applied Energy, 2015, 156: 519-527
508 [30] Kai Wang, Hongwei Wu, Dunjin Wang, Yongsheng Wang, Zhiting Tong, Feng
509 Lin, A.G. Olabi, Experimental Study on a Coiled Tube Solar Receiver under
510 Variable Solar Radiation Condition, Solar Energy, 2015,122: 1080–1090
511 [31] Mawire A., Taole S., 2014. Experimental energy and exergy performance of a
512 solar receiver for a domestic parabolic dish concentrator for teaching purposes.
513 Energy Sustain. Dev. 19:162-9.
514 [32] Macphee D., Dincer I., 2009. Thermal modeling of a packed bed thermal energy
515 storage system during charging. Appl. Therm. Eng. 29:695-705.
516 [33] Petela R., 2003. Exergy of undiluted thermal radiation. Solar Energy, 74:469-88.
517 [34] Moffat RJ. Describing the uncertainties in the experimental results. Exp. Therm.
518 Fluid Sci., 1988; 1:3-17

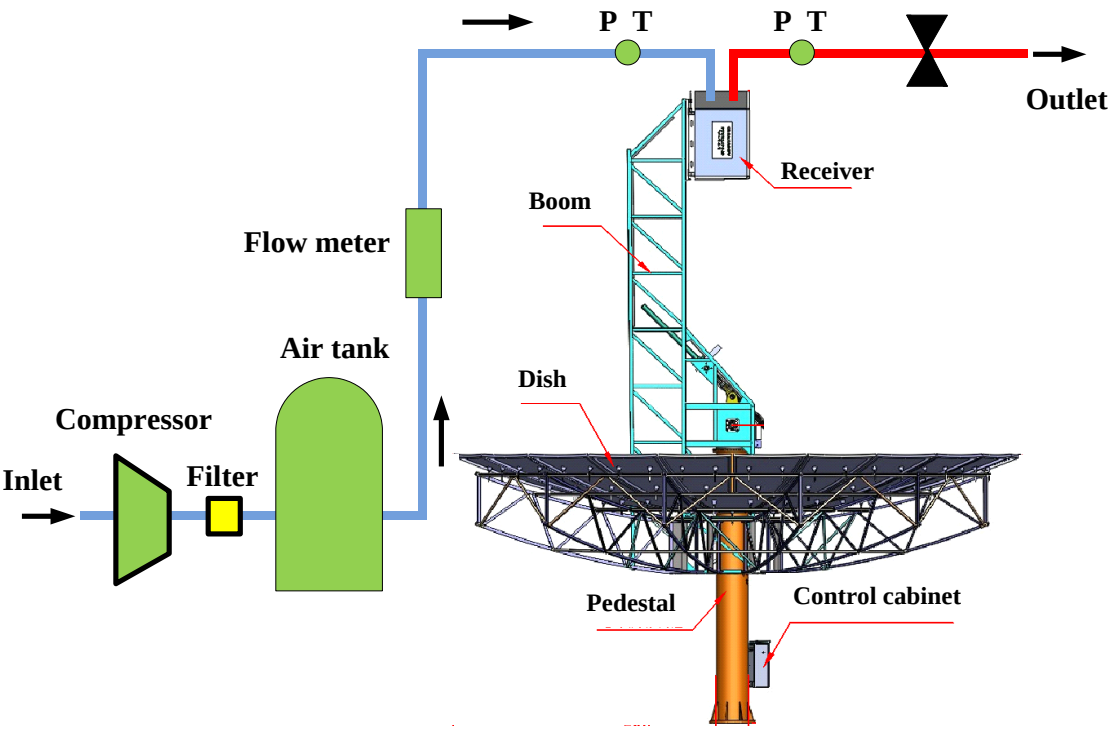

519 [35]

520 [36] **Fig. 1.** Schematic drawing of experimental test rig.

Fig. 2. Parabolic dish.

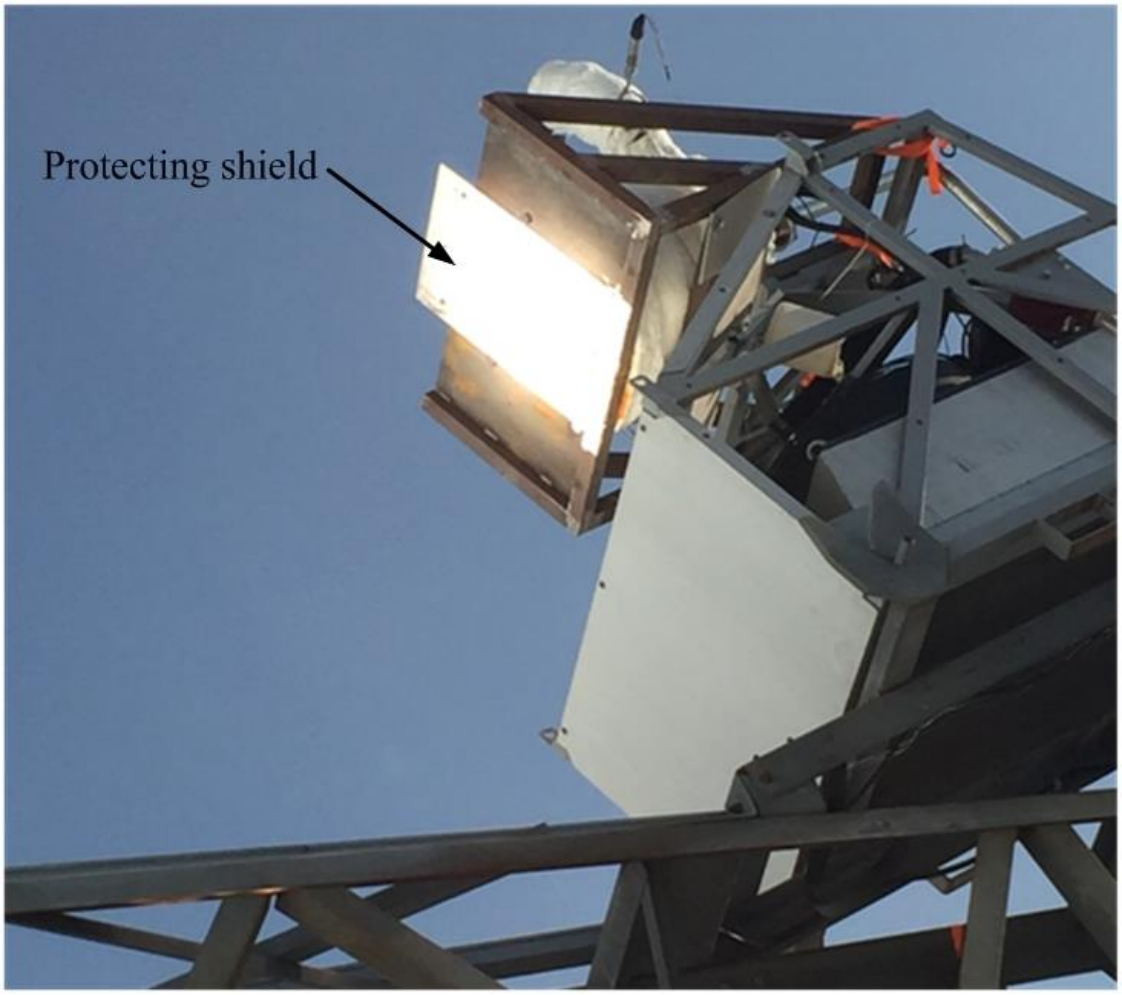

[39]

[40] **Fig. 3.** Protecting shield under the concentrated solar radiation.

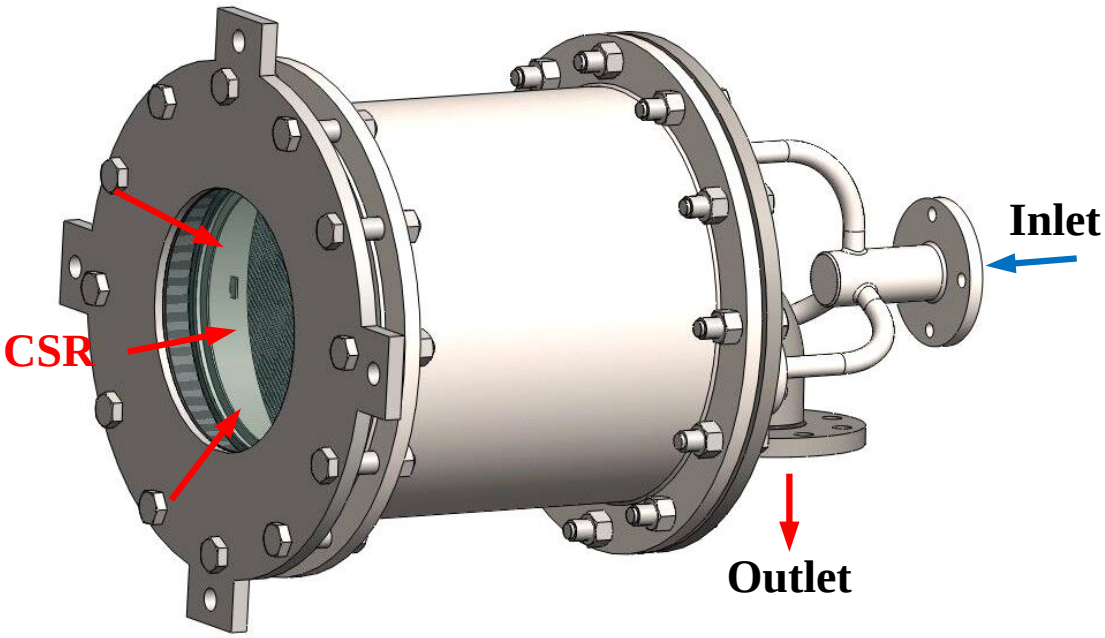

[41]

[42] **(a)**

[43]

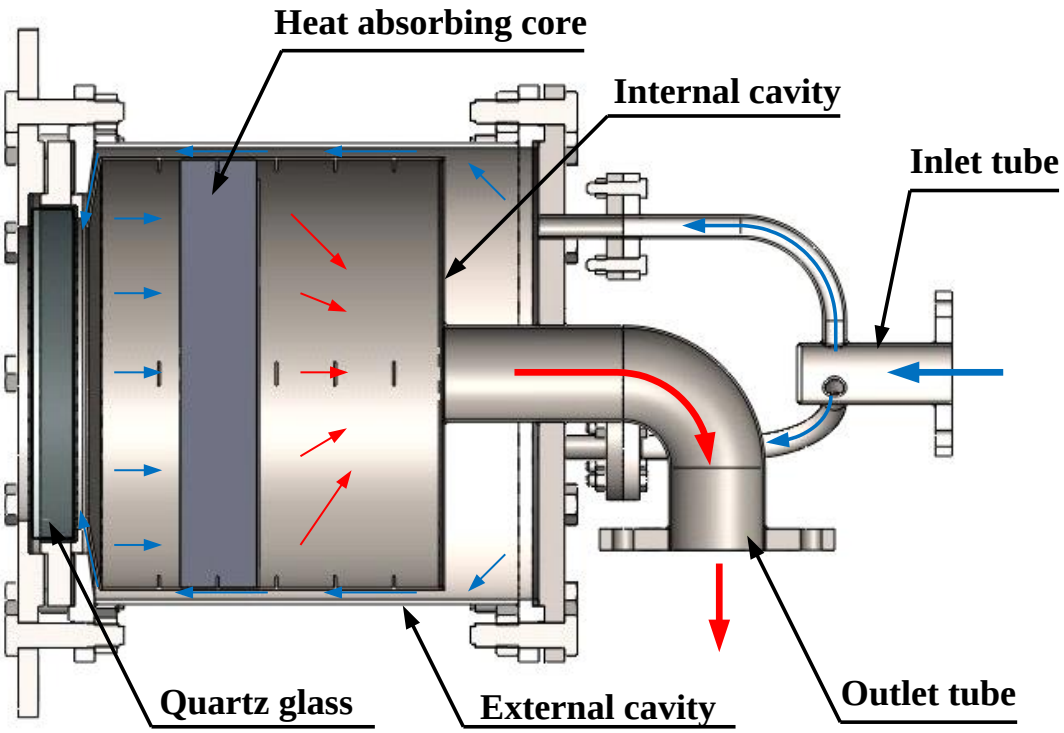

[44]

[45] **(b)**

[46] **Fig. 4.** Pressurized volumetric solar receiver. (a) 3D model, (b) cross sectional view.

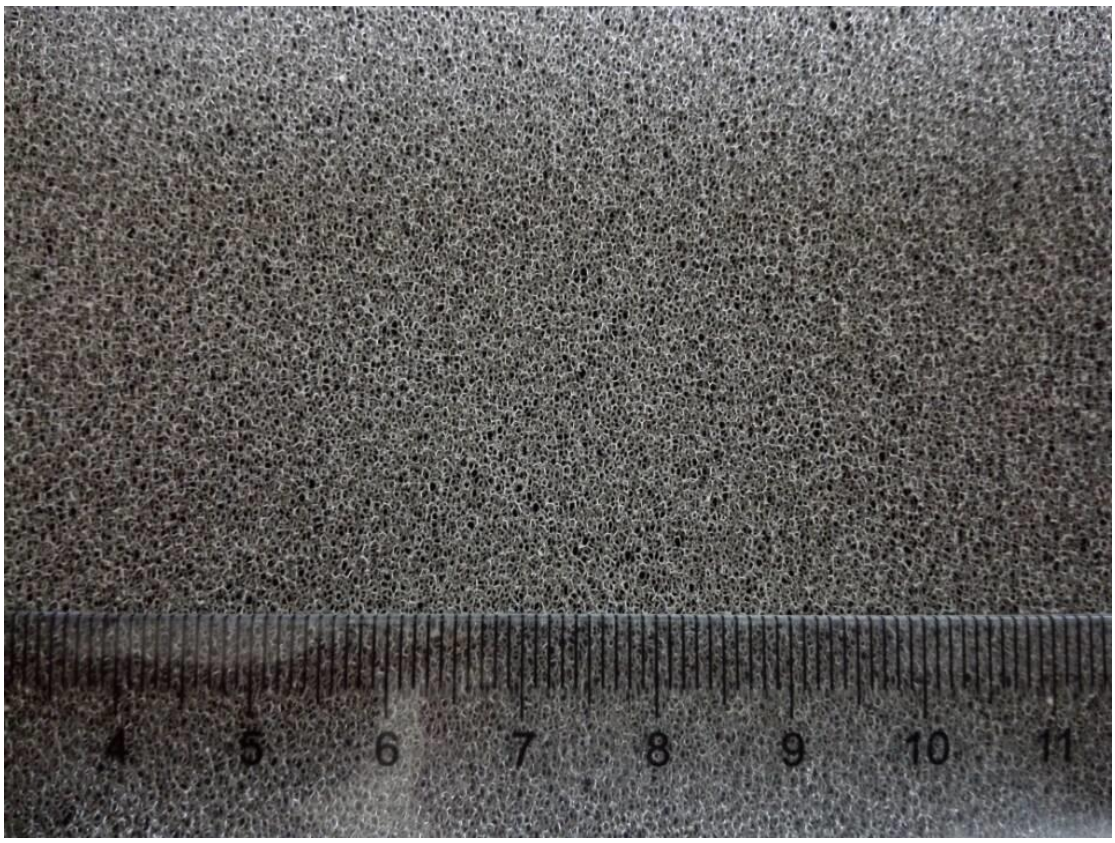

[47]

[48] **Fig.5.** Nickel foam.

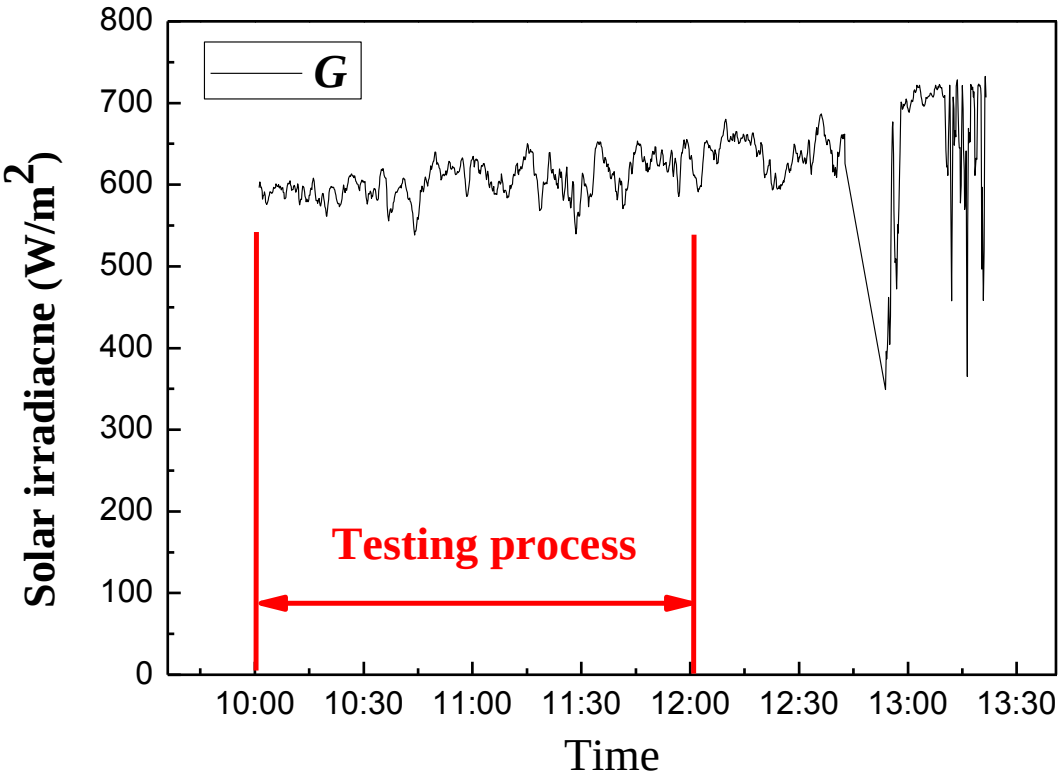

[49]

[50] **Fig. 6.** Solar irradiance data during the day.

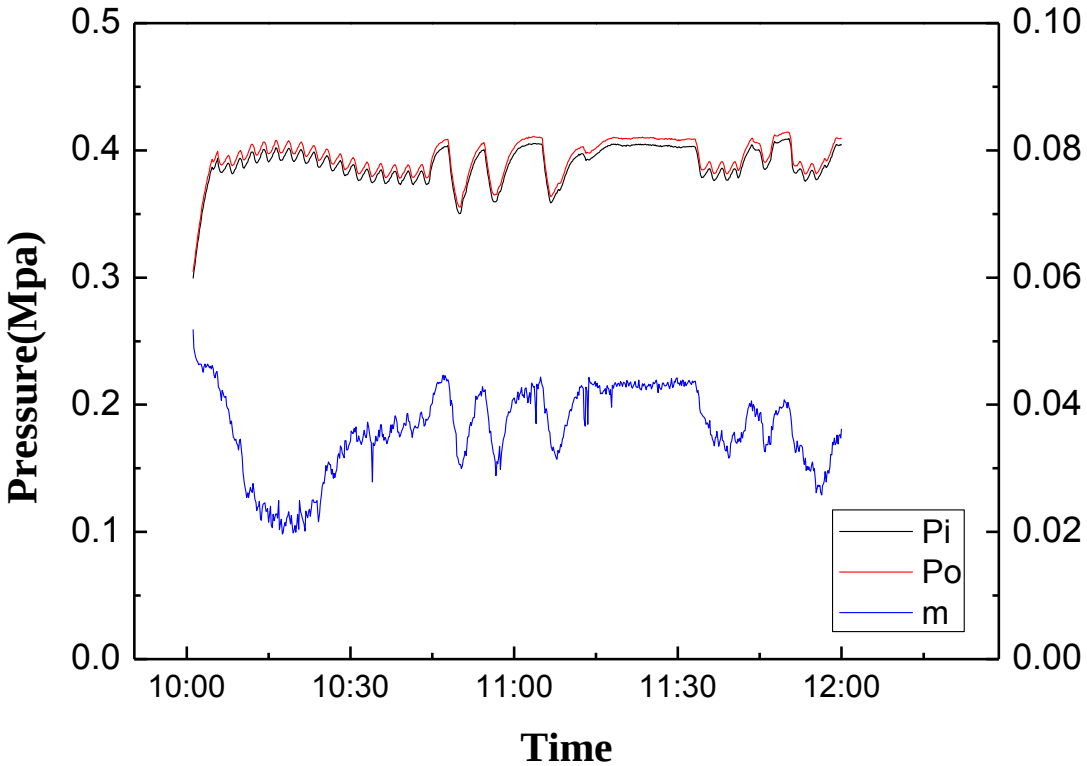

[51]

[52] **Fig. 7.** Variation of the inlet pressure, outlet pressure and mass flow rate.

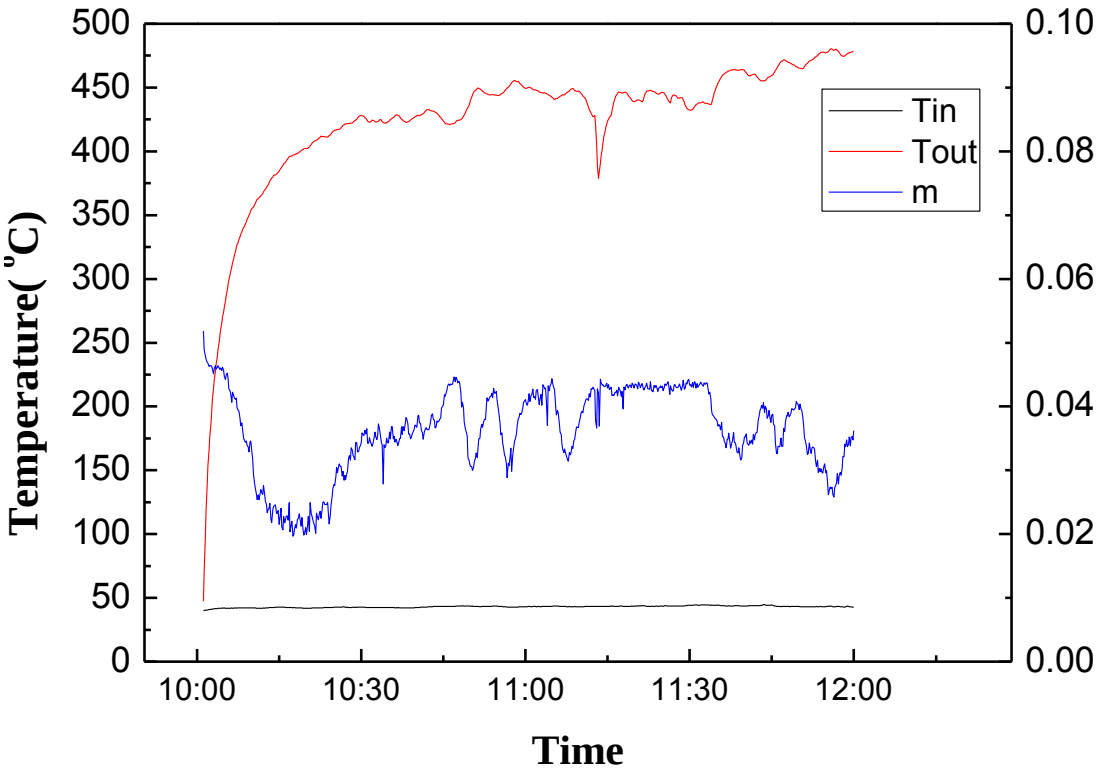

[53]

[54] **Fig. 8.** Variation of the inlet temperature, outlet temperature and mass flow rate.

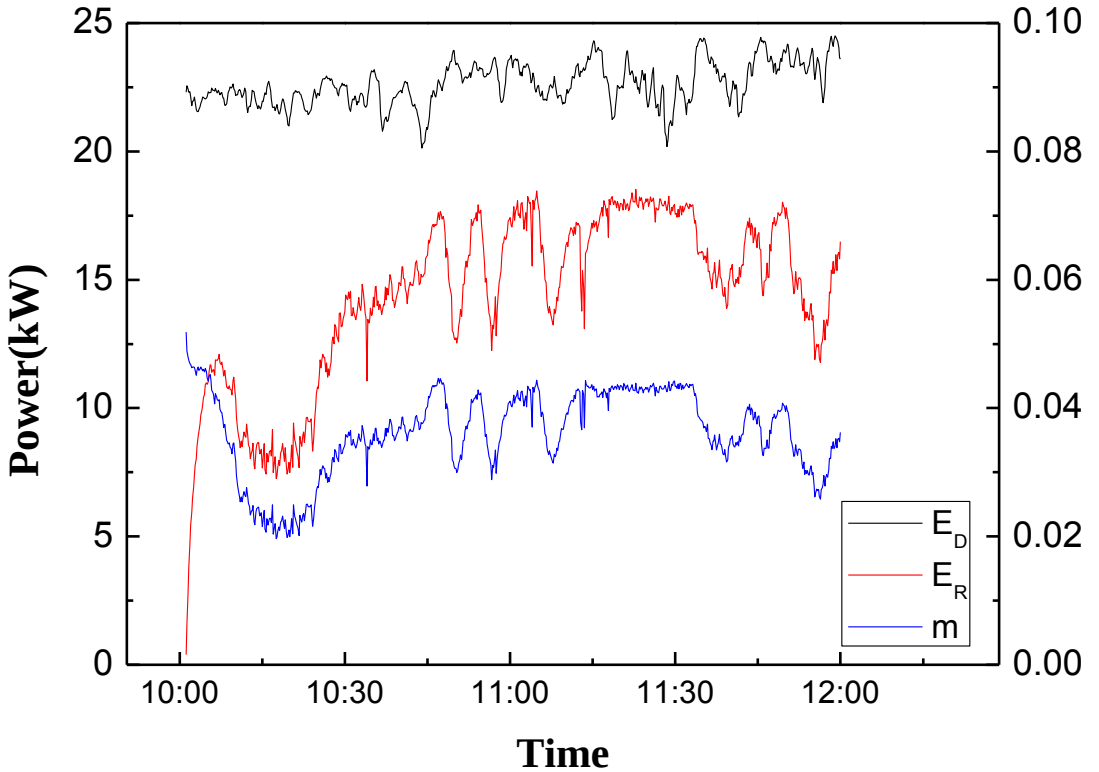

[55]

[56] **Fig. 9.** Variation of the dish power, receiver power and mass flow rate.

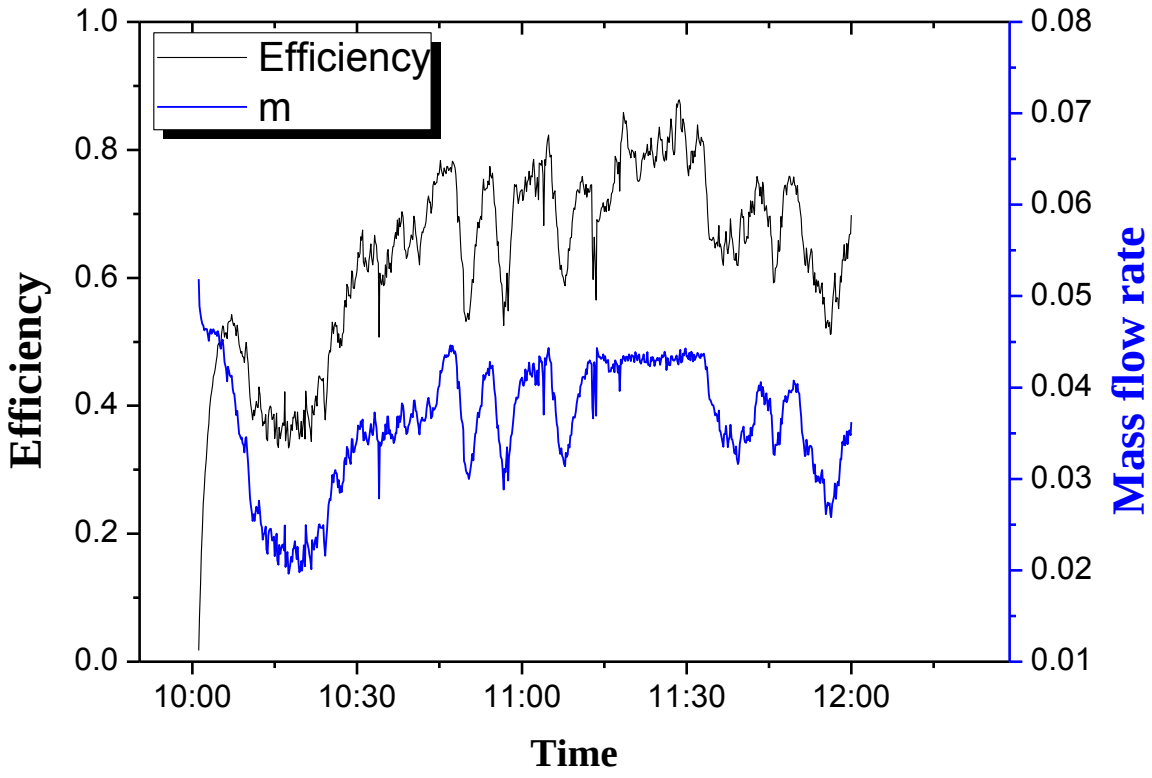

[57]

[58] **(a)**

[59]

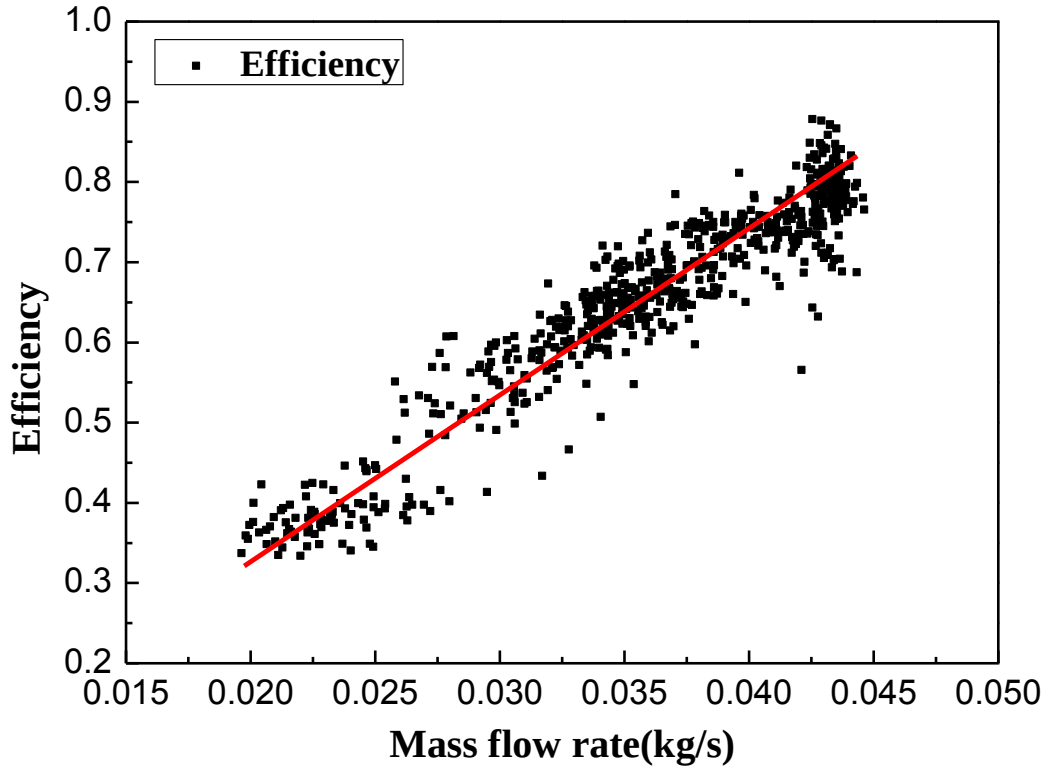

[60]

[61] **(b)**

[62] **Fig. 10.** Efficiency results. (a) during the test period, (b) efficiency vs. mass flow rate.

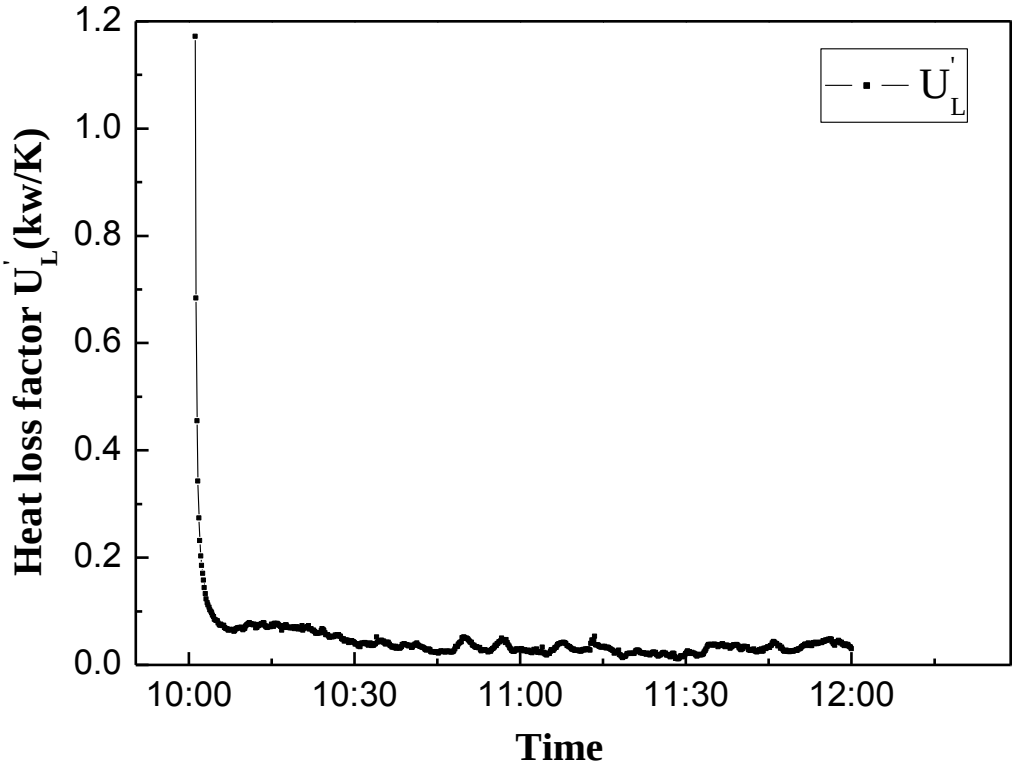

[63]

[64] **Fig. 11.** Heat loss factor profile during the test period.

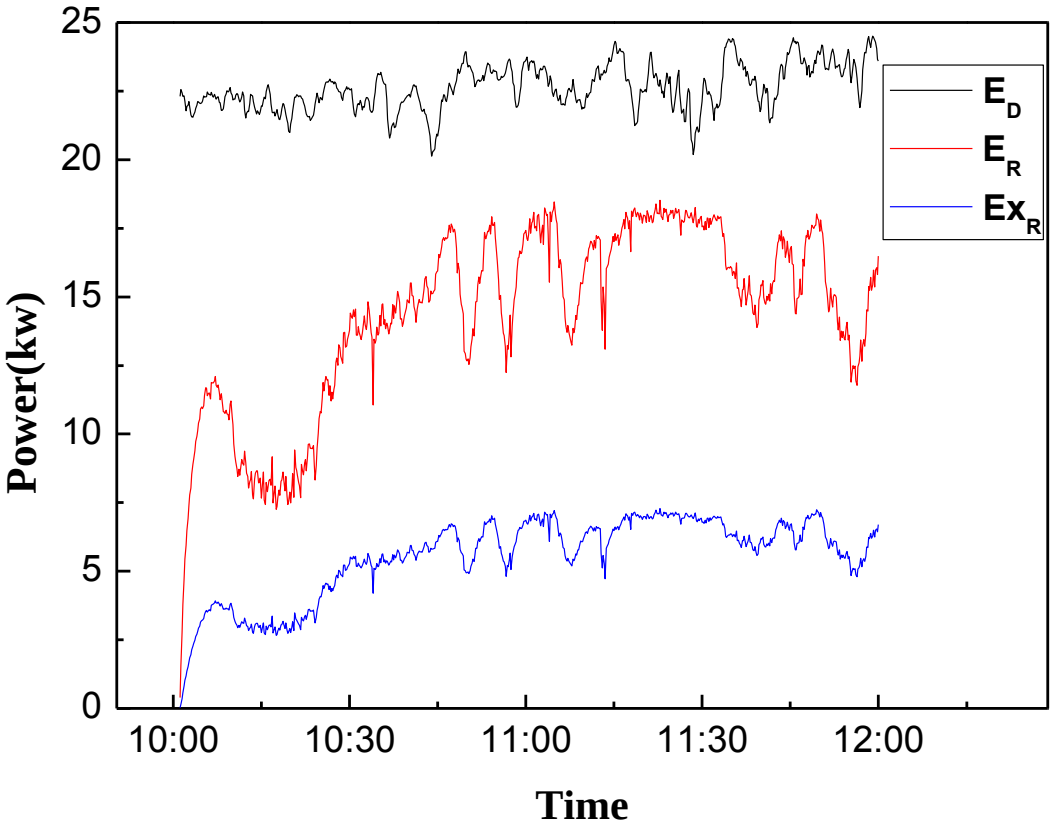

[65]

[66] **Fig. 12.** Variation

of the power for the receiver energy and exergy

[67] during the test period.

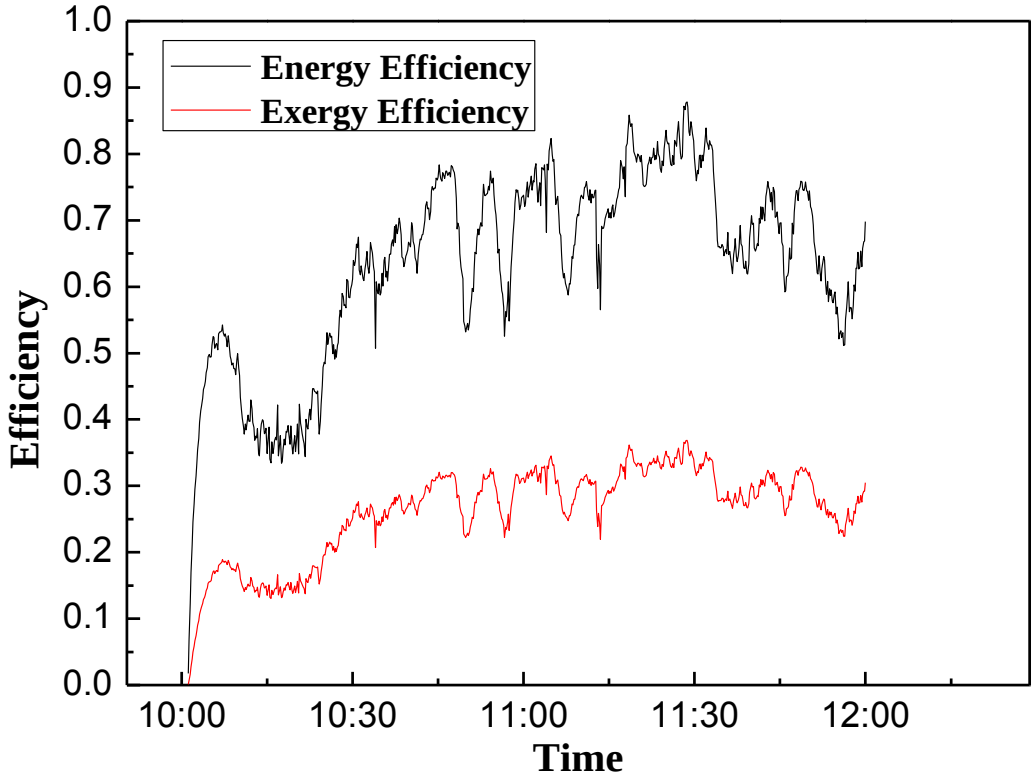

[68]

[69] **Fig. 13.** Energy and Exergy efficiency profile during the test period.

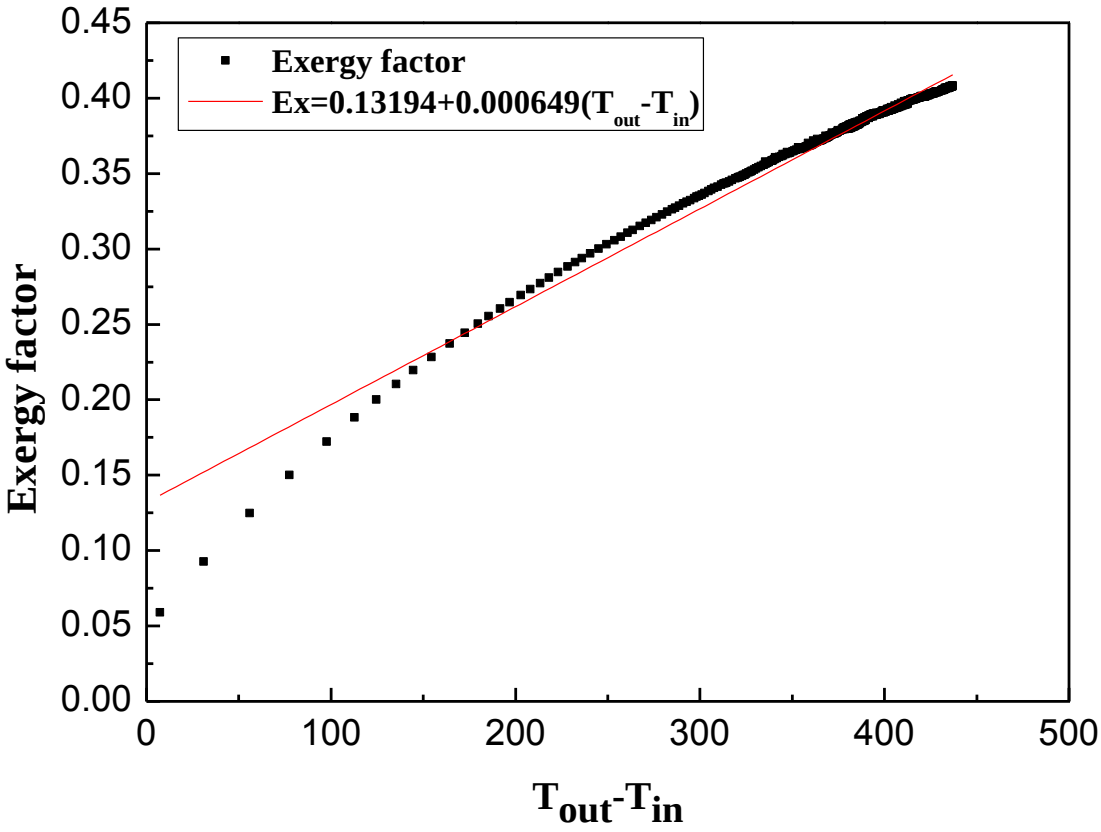

[70]

[71] **Fig. 14.** The effect of temperature difference on the exergy factor.

[72]